Proceedings of IMECE 2004:
2004 ASME International Mechanical Engineering Congress
November 13-19, Anaheim, California

IMECE2004-60969

ADVANCED SIGNAL PROCESSING TECHNIQUES FOR MULTI-DAMAGE DETECTION WITH AN IMPROVED EMBEDDED ULTRASONIC STRUCTURAL RADAR ALGORITHM AND PIEZOELECTRIC WAFER ACTIVE SENSORS

Lingyu Yu, PhD candidate
Mechanical Engineering Department, University of South Carolina
Columbia, SC 29208, USA
(O)803.777.1535
yu3@engr.sc.edu

Victor Giurgiutiu, Associate Professor
Mechanical Engineering Department, University of South Carolina
Columbia, SC 29208, USA
(O)803.777.8018
giurgiut@engr.sc.edu

ABSTRACT

The embedded ultrasonic structural radar (EUSR) algorithm was developed by using piezoelectric wafer active sensor (PWAS) array to detect defects within a large area of a thin-plate specimen. EUSR was verified to be effective for detecting a single crack either at a broadside or at an offside position. However, the damage location was not very precise. This algorithm is improved by using advanced signal processing techniques. The improvement includes: 1) EUSR is able to provide better image of the specimen under monitoring; 2) it is able to detect multiple defects such as several cracks; 3) it is also able to identify different damage types.

This paper starts with an introduction of embedded ultrasonic structural radar algorithm. Then the application of using Hilbert transform for extracting the envelopes of the wave packages is discussed. This can eliminate or reduce the effect of side robes so that EUSR produces better images. The improvement of EUSR detectability is concluded through the comparison to the previous results, followed by the experiments to verify the multi-damage detection of EUSR. Finally, we present the results of how EUSR can distinguish different types of damage. This system is implemented by developing a graphical user-friendly interface program in LabView. We conclude with a description of our vision for an even more powerful EUSR for structural health monitoring and embedded nondestructive evaluation.

KEYWORDS

Signal processing, Hilbert transform, SHM, damage detection

INTRODUCTION

Embedded nondestructive evaluation (NDE) is an emerging technology that will allow transitioning the methods of conventional ultrasonic to embedded systems structural health monitoring (SHM) such as those envisioned for the Integrated Vehicle Health Management (IVHM). SHM for IVHM-requires the development of small, lightweight, inexpensive, unobtrusive, minimally invasive sensors to be embedded in the airframe with minimum weight penalty and at affordable costs. Such sensors should be able to scan the structure and identify the presence of defects and incipient damage.

Current ultrasonic inspection of thin wall structures (e.g., aircraft shells, storage tanks, large pipes, etc.) is a time consuming operation that requires meticulous through-the-thickness C-scans over large areas. One method to increase the efficiency of thin-wall structures inspection is to utilize guided waves (e.g., Lamb waves) instead of the conventional pressure waves. Guided waves propagate along the mid-surface of thin-wall plates and shallow shells. They can travel at relatively large distances with very little amplitude loss and offer the advantage of large-area coverage with a minimum of installed sensors. Guided Lamb waves have opened new opportunities for cost-effective detection of damage in aircraft structures, and a large number of papers have recently been published on this subject. Traditionally, guided waves have been generated by impinging the plate obliquely with a tone-burst from a relatively large ultrasonic transducer. Snell's law ensures mode conversion at the interface, hence a combination of pressure and shear waves are simultaneously generated into the thin plate. However, conventional Lamb-wave probes (wedge and comb transducers) are relatively too heavy and expensive to consider for widespread deployment on an aircraft structure as part of a SHM system. Hence, a different type of sensors than the conventional ultrasonic transducers is required for the SHM systems.

1. THE EMBEDDED ULTRASONIC STRUCTURAL SENSOR (EUSR) ALGORITHM AND PREVIOUS WORK

The principle of operation of the embedded ultrasonic structural radar (EUSR) is derived from two general principles: (1) The

principle of guided Lamb wave generation with piezoelectric wafer active sensors (PWAS); (2) The principles of conventional phased-array radar.

The guided Lamb waves generated by PWAS have the important property that they stay confined inside the walls of a thin-wall structure, and hence can travel over large distances. In addition, the guided wave can also travel inside curved walls, which makes them ideal for applications in the ultrasonic inspection of aircraft, missiles, pressure vessel, oil tanks, pipelines, etc. This has been proved by our curvature experiment. Lamb waves can exist in a number of dispersive modes. However, through smoothed tone-burst excitation and frequency tuning, it is possible to confine the excitation to a particular Lamb wave mode, of carrier frequency *fc*, wave speed c, and wave length $\lambda = c/f_c$. Hence, the smoothed tone-burst signal generated by one PWAS is of the form:

$$s_T(t) = s_0(t)\cos 2\pi f_c t \tag{1}$$

where $s_0(t)$ is a short-duration smoothing window that is applied to the carrier signal of frequency *fc* between 0 and *tp*.

The principle of conventional phased-array radar is applied to the PWAS-generated guided waves, assuming a uniform linear array of *M* sensors (PWAS), with each PWAS acting as a pointwise omni-directional transmitter and receiver. The PWAS in the array are spaced at the distance *d*, which is assumed much smaller than the distance *r* to a generic, far-distance point, *P*. Since *d* << *r*, the rays joining the sensors with the point P can be assimilated with a parallel fascicle, of ϕ . Therefore, for the m^{th} PWAS, the distance will be shorted by $m(d\cos\phi)$. If all the PWAS are fired simultaneously, the signal from the m^{th} PWAS will arrive at P quicker by $\Delta_m(\phi) = m(d\cos\phi)/c$. Yet, if the PWAS are not fired simultaneously, but with some individual delays, δ_m , *m* = 0,1,…,*M*-1, then the total signal received at point P will be:

$$s_P(t) = \frac{1}{\sqrt{r}}\sum_{m=0}^{M-1} s_T\left(t - \frac{r}{c} + \Delta_m(\phi) - \delta_m\right) \tag{2}$$

$1/r$ represents the decrease in the wave amplitude due to the omni-directional 2-D radiation, and r/c is the delay due to the travel distance between the reference PWAS (*m* = 0) and the point P. (Here wave-energy conservation, i.e., no dissipation, is assumed.)

Transmitter beamforming: if we have $\delta_m = m\Delta(\phi)$, then Equation (2)becomes:

$$s_P(t) = M\cdot\frac{1}{\sqrt{r}} s_T\left(t - \frac{r}{c}\right) \tag{3}$$

That's to say, there is an M times increase in the signal strength with respect to a simple sensor. This leads directly to the beamforming principle that if $\delta_m = md\cos(\phi_0)/c$, and since $\Delta_m = md\cos(\phi)/c$, then constructive interference (beamforming) takes place when $\cos(\phi) = \cos(\phi_0)$, i.e. at angles $\phi = \phi_0$ and $\phi = -\phi_0$. Thus, the forming of a beam at angles ϕ_0 and $-\phi_0$ is achieved through delays in the firing of the sensors in the array.

Receiver beamforming: if the point P is an omni-directional source at azimuth ϕ_0 , then the signals received at the m^{th} sensor will arrive quicker by $m\Delta_0\phi = md\cos(\phi_0)/c$. Hence, we can synchronize the signals received at all the sensors by delaying them by:

$$\delta_m(\phi_0) = m\frac{d}{c}\cos(\phi_0) \tag{4}$$

Pulse-echo method: Assume that a target exists at azimuth ϕ_0 and distance R. The transmitter beamformer is sweeping the range in increasing angles ϕ and receives an echo when $\phi = \phi_0$. The echo will be received on all sensors, but the signals will not be synchronized. To synchronize the sensors signals, the delays $\delta_m(\phi_0) = md\cos(\phi_0)/c$ need to be applied.

The original signal is:

$$s_P(t) = \frac{M}{\sqrt{R}} s_T\left(t - \frac{2R}{c}\right) \tag{5}$$

At the target, the signal is backscattered with a backscatter coefficient, A. Hence, the signal received at each sensor will be:

$$\frac{A\cdot M}{R} s_T\left(t - \frac{2R}{c} + \Delta_m(\phi)\right) \tag{6}$$

The receiver beamformer assembles the signals from all the sensors with the appropriate time delays:

$$s_R(t) = \frac{A\cdot M}{R}\sum_{m=0}^{M-1} s_T\left(t - \frac{2R}{c} + \Delta_m(\phi) - \delta_m\right) \tag{7}$$

Constructive interference between the received signals is achieved when $\delta_m = md\cos(\phi_0)/c$. Thus, the assembled receive signal will be again boosted *M* times, with respect to the individual sensors:

$$s_R(t) = \frac{A\cdot M^2}{R}\sum_{m=0}^{M-1} s_T\left(t - \frac{2R}{c}\right) \tag{8}$$

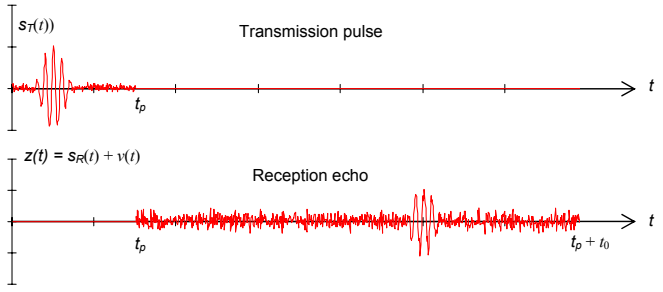

Figure 1 the transmitted signal and the received signal

In general, a target crack is unknown, i.e. the target location is unknown. Since we use the polar coordinates in the radar system, the location of an unknown target is defined by the angle ϕ_0 . The coarse estimation of ϕ_0 is implemented by using the ϕ_0 sweeping method. EUSR will scan through 0º to 180º by incrementing ϕ_0 by 1º each time, until the maximum received

energy is obtained. $\max E_R(\phi_0)$ is the maximum received energy by the definition:

$$E_R(\phi_0) = \int_{t_p}^{t_p+t_0} \left| s_R(t,\phi_0) \right|^2 dt \qquad (9)$$

Figure 1 is an example of the transmitted signal and received signal pair captured in our experiment.

The specimens we used in the lab are 4-feet long, 1-mm thick square aluminum plates with an 8-element PWAS array at the center. The layout is shown in Figure 2 (a). Figure 2 (b) is the experiment setup.

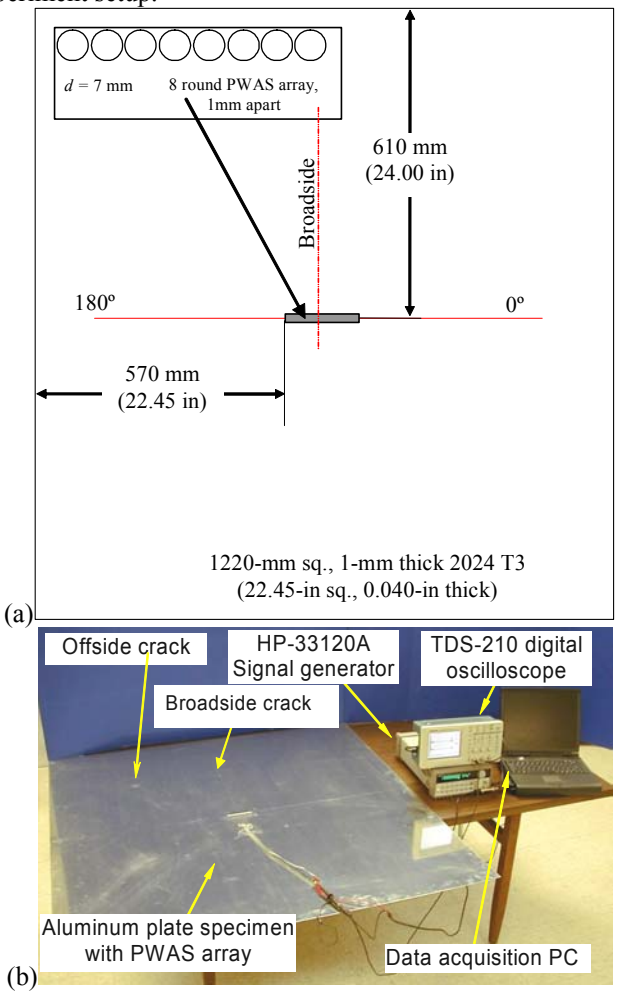

Figure 2 EUSR experiment with the 8 element PWAS array: (a) specimen layout; (b) experiment setup

In our experiment, broadside position is defined to be perpendicular to the PWAS array (see Figure 3 a) and the offside position is anywhere between the 0º and 180º but the broadside position (see Figure 4 a). The cracks are simulated by through-plate cracks 14 mm long and 0.5 mm wide.

We have done previous proof-of-concept work by using EUSR to verify its ability for detecting a single crack at either broadside or offside position on a thin-plate specimen. Figure 3 (b) and Figure 4 (b) are the 2D display of single crack inspection by using the previous EUSR. The offside position is at angle 137º.

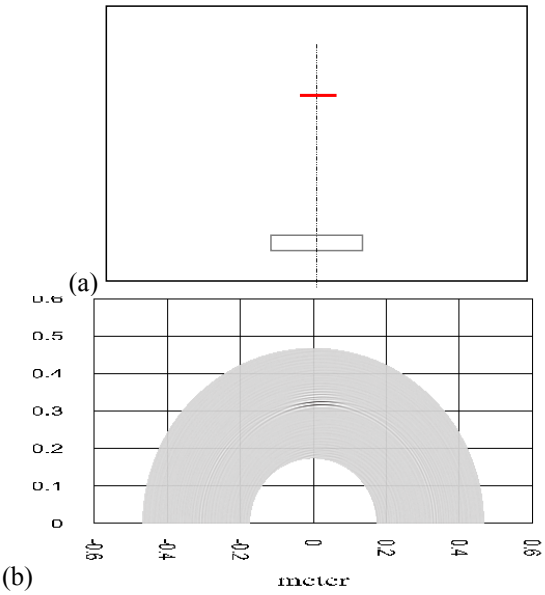

Figure 3 single broadside crack detection with previous EUSR: (a) schematic; (b) EUSR GUI mapped image

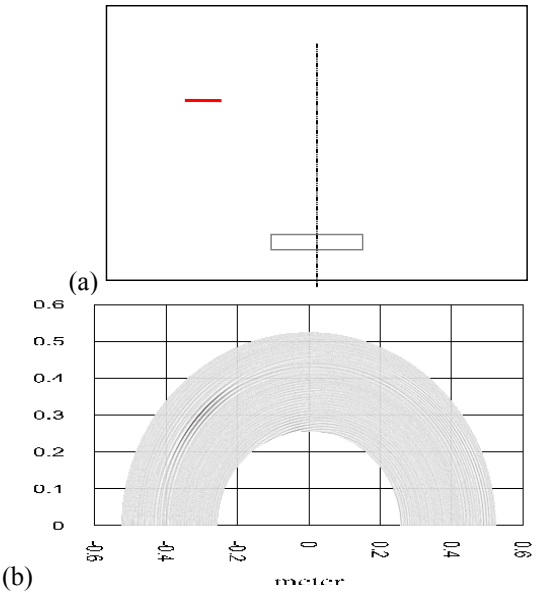

Figure 4 single offside crack detection with previous EUSR: (a) schematic; (b) EUSR GUI mapped image

2. AN IMPROVED EUSR BY USING THE HILBERT TRANSFORM

From the specimen inspection plots, we can see that though they can generally locate the damage, they are far than close to the real cracks. We expected to find a solution to improve the image quality and precision.

One thing we noticed is, our echoes from the damage do not have single peaks due to the dispersion property or some reasons. We need to find a way to get echoes close to the theoretical ones, having single peaks. The method being explored is the Hilbert transform, which is able to extract the envelope of a curve. The envelope is a curve or surface that is

tangent to every one of a family of curves or surfaces. Envelope extracts the amplitude of a periodic signal. It can be used to simplify the process of detecting the time of arrival for the wave packets in our EUSR system. In the EUSR, the envelope of the signal is extracted by applying Hilbert transform to the cross correlation signal.

The Hilbert transform is defined as:

$$H(x(t)) = -\frac{1}{\pi}\int_{-\infty}^{+\infty}\frac{x(\tau)}{t-\tau}d\tau \qquad (10)$$

Hilbert transform is often used to construct a complex signal:

$$\tilde{x}(t) = \tilde{x}_{\mathrm{Re}}(t) + i\cdot\tilde{x}_{\mathrm{Im}}(t) \qquad (11)$$

Where

$$\begin{aligned}\tilde{x}_{\mathrm{Re}}(t) &= x(t)\\ \tilde{x}_{\mathrm{Im}}(t) &= H\left(x(t)\right)\end{aligned} \qquad (12)$$

The real part of the constructed signal, $\tilde{x}_{\mathrm{Re}}(t)$, is the original data $x(t)$, while the imaginary part $\tilde{x}_{\mathrm{Im}}(t)$ is the Hilbert transform of $x(t)$. Actually, the imaginary part is a version of the original real sequence after a 90° phase shift. Thus, the Hilbert transformed signal has the same amplitude and frequency content as the original real signal and includes phase information that depends on the phase of the original signal. The magnitude of each complex value has same the amplitude as the origin signal. Therefore, we can say that the magnitude of the analytical signal is the envelope of the original signal. Just by observing the envelope signal, the wave packages can be easily recognized. Figure 5 is an example showing how Hilbert transform extracts the envelope of a tone-burst signal.

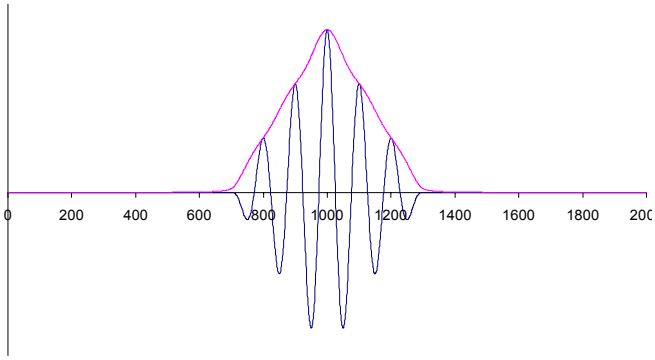

Figure 5 a tone-burst signal and its envelope extracted by using Hilbert transform

Therefore, we applied the Hilbert transform to our EUSR system after the EUSR data was constructed to extract these data's envelopes, such that we can achieve a smooth curve with a single peak, eliminating the previous spike effect. The processing results in Figure 6 show that this process does result in a more distinct representation of echoes from the cracks and therefore a much clearer indication of the cracks. Compared with results in Figure 3 and Figure 4, Figure 6 images have fewer ripples and spikes, and better resolution, much closer to the cracks' real size.

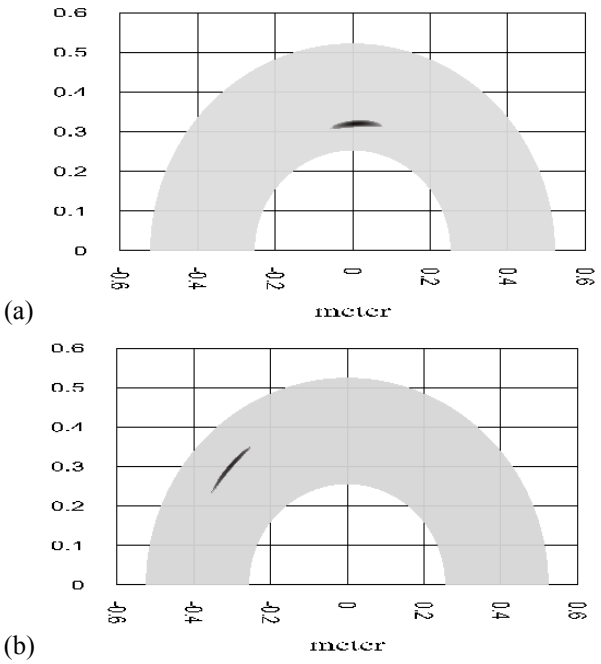

Figure 6 single crack detection with the improved EUSR: (a) broadside crack detection; (b) offside crack detection

3. EUSR MULTI-CRACK DETECTION EXPERIMENTS

Our previous work has proved EUSR's ability to detect a single through plate crack in a thin plate. The new experiments are designed to verify EUSR is also able to detect multiple cracks and pin-holes as well. The experiments that we have gone through including:

- Broadside crack with certain slope
- Two aligned offside cracks
- Three aligned cracks, two offside cracks and one horizontal broadside crack
- Three aligned cracks, two offside cracks and one perpendicular broadside crack
- Pin holes from 0.5mm, 1mm, 1.57mm and 2mm

3.1. Broadside crack with certain slope

The specimen #7 has a broadside crack with the 20-mm crack dimension, but 30º to the horizontal. The experiment result in Figure 7 shows that EUSR is able to indicate the slope. The plot is a little different from the horizontal crack showing in Figure 6 a). In the future, we will do further experimentation to find out the minimum slope that EUSR is sensitive and able to indicate, and compare the results of different slops.

3.2. Two aligned offside cracks

The specimen #6 has two symmetrical offside cracks at 63º and 117º positions, respectively. Figure 8 shows the EUSR inspection result.

One thing has to be mentioned is, for some reason, the two cracks are actually not exactly symmetrical to each other as the original design. They are 3 mm from each vertically. However, the 2D inspection plot picked out such a difference, and we can see the two cracks are in different circles (having different

vertical distance to the PWAS array). We can say that EUSR is able to even pick up that small difference (Figure 8).

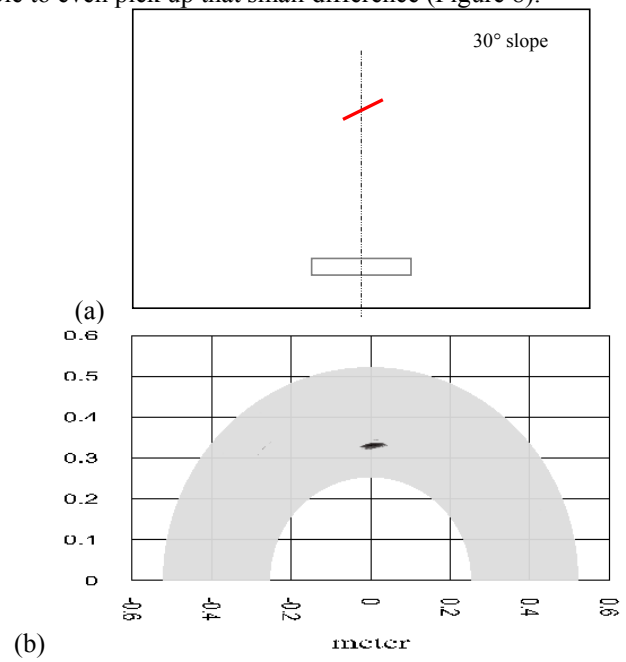

Figure 7 the broadside crack having 30º slopes: (a) schematic; (b) EUSR 'GUI mapped image

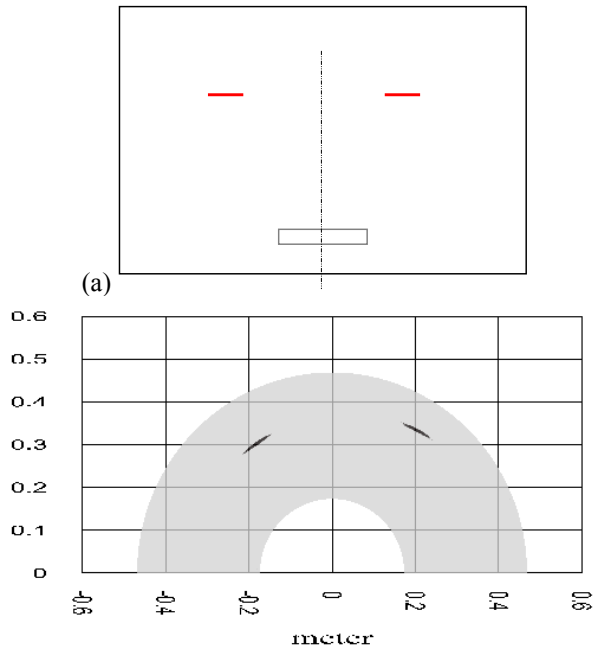

Figure 8 the two symmetrical offside cracks at 63º and 137º, respectively: (a) schematic; (b) EUSR GUI mapped image

3.3. Pin-holes

As another type of through-plate damage, we worked to verify EUSR ability to detect pin holes and find out the minimum detectable pin-hole size. The experiment will go through the pin holes with 0.5mm, 1mm, 1.57mm and 2mm.

The experiment results show that we failed with the pin-holes with 0.5mm diameter and 1mm diameter. But it can detect the pin hole with 1.57mm diameter. See Figure 9 (a). The tiny dot at the broadside position is the simulation of the pin hole in the 2D plot. The Figure 9 (c) shows the result of the pin-hole with 2 mm diameter, which is much clearer than the pin-hole with 1.57 mm diameter in Figure 9 (b).

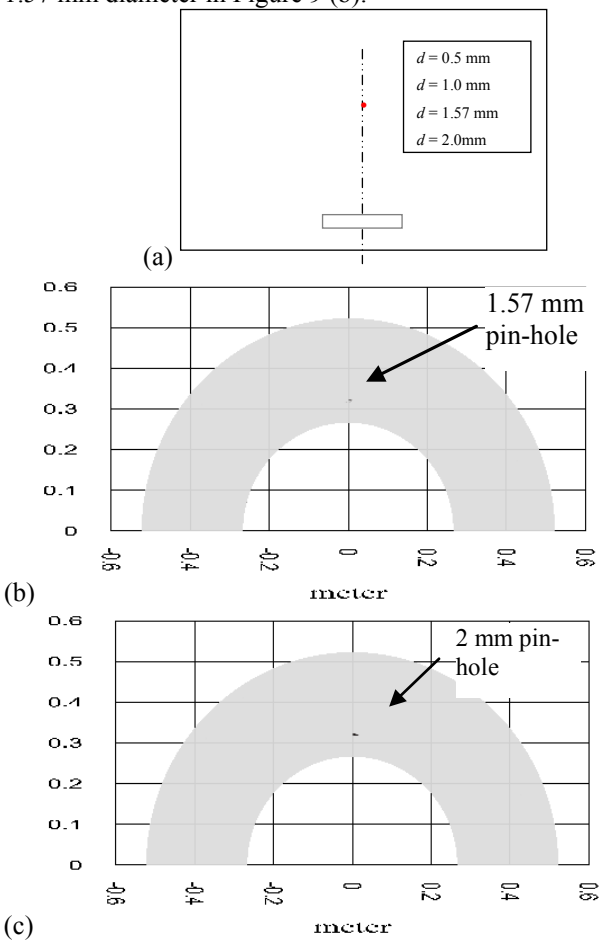

Figure 9 pin-holes: (a) schematic; (b) EUSR GUI mapped image of the minimum detectable pin-hole with 1.57mm diameter; (c) EUSR GUI mapped image of pin-hole with 2mm diameter

4. NEXT STEP: THREE ALIGNED CRACKS

In the three aligned cracks experiments, we have two designs. Both designs have two offside horizontal cracks at 63º and 137º positions. Design 1 has a broadside crack parallel to the PWAS array while design 2 has a broadside crack perpendicular to the PWAS array. See Figure 10.

Design 1: the horizontal broadside crack (Figure 10 a)

Design 2: the vertical broadside crack (Figure 10 b)

To this moment, EUSR algorithm is able to detect the presence of the three cracks in the A-scan signal, but not in the mapped EUSR image for the three cracks experiments. The reason for this may be that the broadside crack reflects more energy than the offside cracks and therefore the energy reflected from the perpendicular crack dominates the EUSR image. For the design

2, recalling the result we have got from the pin-hole experiments, the minimum hole size that can be detected by EUSR is 1.57 mm. Therefore the crack in the design 2 may be too tiny to be detected.

In our next stage, we will apply the signal processing techniques and try signal analysis methods to improve the results. And we will gradually enlarge the vertical crack to find out the smallest dimension to be detected and further verify EUSR.

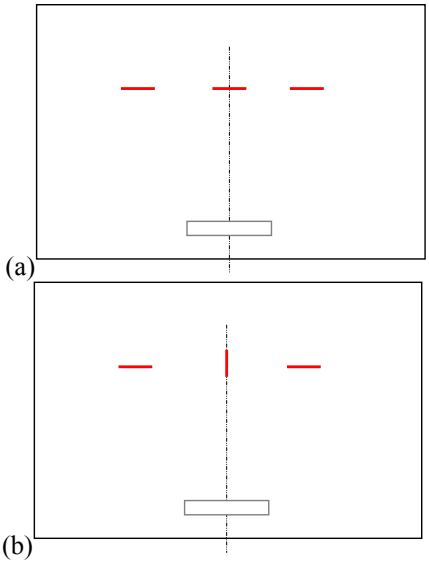

Figure 10 three aligned cracks: (a) schematic of the horizontal broadside crack; (b) schematic of the vertical broadside crack

5. DISCUSSIONS AND CONCLUSIONS

This paper has presented the applications of signal processing techniques to the existing embedded ultrasonic structural radar (EUSR) algorithm using piezoelectric wafer active sensors. After presenting the general principles of the EUSR algorithm and the previous work, we discussed how we use the Hilbert transform to extract the signal envelopes to improve the efficiency and reliability of existing EUSR. A series of experiments are conducted to verify the EUSR's ability to detect multi-cracks, including: (a) broadside crack with certain slope; (b) two horizontal aligned cracks; (c) pin-holes. We have achieved the inspection plots of the cracks from the specimens under monitoring.

For the three horizontal aligned cracks with two types of middle crack cases, we envision to apply signal processing techniques and enlarge the vertical crack dimension in our next step coming soon. Figure 11 shows the data flow of the EUSR.

ACKNOWLEDGMENTS

Support from the Air Force Research Lab through UTC Contract #03-S470-033-C1 of F33615-01-D-5801 is thankfully acknowledged.

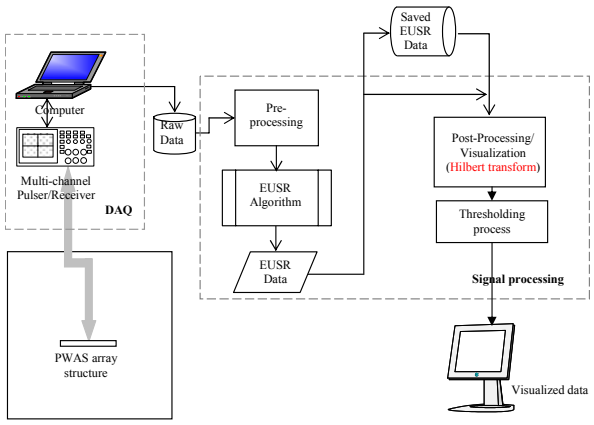

Figure 11 data flow of the damage detection by using the improved EUSR algorithm

REFERENCES

[1] Kim, H.; Melhem, H. "Fourier and Wavelet Analysis for Fatigue Assessment of Concrete Beams" Experimental Mechanic, pp.131-140, Jun. 2003

[2] Rioul, O.; Vetterli, M. "Wavelets and Signal Processing" IEEE SP magazine Oct. 1991 pp.14-35

[3] Boggess, A.; Narcowich, F. A First Course in Wavelets with Fourier Analysis Prentice-Hall, Inc. 2001 Upper Saddle River, NJ 07458

[4] Elliott, D. Handbook of Digital Signal Processing, Engineering Applications Rockwell International Corporation, Anaheim, CA92101

[5] Tong, C.; Figueroa, F. "A Method for Short or Long Range Time-of-Flight Measurements Using Phase-Detection With an Analog Circuit" IEEE Transactions on Instrumentation and Measurement, Vol. 50, NO. 5, Oct. 2001

[6] Chao, Y., and Rose, J. L. (2000) "An Elastodynamic Hybrid Boundary Element Study for Elastic Guided Wave Interactions with a Surface Breaking Defect", International Journal of Solids and Structures, Vol. 37, 2000, pp. 4013-4124

[7] Giurgiutiu, V.; Bao, J. (2002) "Embedded Ultrasonic Structural Radar for the Nondestructive Evaluation of Thin-Wall Structures" Proceedings of the 2002 ASME International Mechanical Engineering Congress, November 17-22, 2002, New Orleans, LA, paper # IMECE2002-39017

[8] Diaz Valdez, S. H., and Soutis, C. (2000) "Health Monitoring of Composites Using Lamb Waves Generated by Piezoelectric Devices", Plastics, Rubber and Composites, Vol. 29, No. 9, 2000

[9] Kay, S. Fundamentals of Statistical Signal Processing, Detection Theory, Prentice Hall PTR 1998, Upper Saddle River, NJ 07458

[10] Yu, L.; Bao, J.; Giurgiutiu, V. "Signal Processing Techniques for Damage Detection with Piezoelectric Wafer Active Sensors and Embedded Ultrasonic Structural Radar", SPIE's 11th Annual International Symposium on Smart Structures and Materials and 9th Annual International Symposium on NDE for Health Monitoring and Diagnostics, 14-18 March 2004, San Diego, CA, paper # 5391-52